nature medicine

β-catenin confers resistance to PI3K and AKT inhibitors and subverts FOXO3a to promote metastasis in colon cancer

Stephan P Tenbaum[1,14], Paloma Ordóñez-Morán[2,13,14], Isabel Puig[1,14], Irene Chicote[1], Oriol Arqués[1], Stefania Landolfi[3], Yolanda Fernández[4], José Raúl Herance[5], Juan D Gispert[5], Leire Mendizabal[6], Susana Aguilar[7,8], Santiago Ramón y Cajal[3], Simó Schwartz Jr[4], Ana Vivancos[6], Eloy Espín[9], Santiago Rojas[5], José Baselga[10,11], Josep Tabernero[12], Alberto Muñoz[2] & Héctor G Palmer[1]

The Wnt–β-catenin and PI3K-AKT-FOXO3a pathways have a central role in cancer. AKT phosporylates FOXO3a, relocating it from the cell nucleus to the cytoplasm, an effect that is reversed by PI3K and AKT inhibitors. Simultaneous hyperactivation of the Wnt–β-catenin pathway and inhibition of PI3K-AKT signaling promote nuclear accumulation of β-catenin and FOXO3a, respectively, promoting cell scattering and metastasis by regulating a defined set of target genes. Indeed, the anti-tumoral AKT inhibitor API-2 promotes nuclear FOXO3a accumulation and metastasis of cells with high nuclear β-catenin content. Nuclear β-catenin confers resistance to the FOXO3a-mediated apoptosis induced by PI3K and AKT inhibitors in patient-derived primary cultures and in corresponding xenograft tumors in mice. This resistance is reversed by XAV-939, an inhibitor of Wnt–β-catenin signaling. In the presence of high nuclear β-catenin content, activation of FOXO3a by PI3K or AKT inhibitors makes it behave as a metastasis inductor rather than a proapoptotic tumor suppressor. We show that it is possible to evaluate the β-catenin status of patients' carcinomas and the response of patient-derived cells to target-directed drugs that accumulate FOXO3a in the nucleus before deciding on a course of treatment. We propose that this evaluation could be essential to the provision of a safer and more effective personalized treatment.

Colon cancer is a leading cause of death worldwide[1]. Although surgical resection combined with adjuvant therapy is efficient at the early stages of disease, subsequent relapse and metastasis often occur. At these advanced stages, resistance to conventional therapies is frequent and treatments are ineffective[2]. To overcome this resistance, a new generation of target-directed drugs is being tested in clinical trials. Therefore, a better understanding of the molecular mechanisms responsible for patients' responses to these drugs is crucial to identify new predictive biomarkers and facilitate treatment decisions.

Abnormal activation of the wingless related MMTV integration site (Wnt)–β-catenin pathway by mutations is responsible for the initiation of more than 90% of colon cancers[3]. As a result, β-catenin accumulates in the nucleus, binds the T cell factor (TCF) or lymphoid enhancer factor (LEF) transcription factors and induces the expression of Wnt target genes that have key roles in tumor progression[4]. We and others have reported that binding of β-catenin to different transcription factors enhances the expression of alternative sets of target genes[5–7]. Forkhead box O3 (FOXO3a) is one of those transcription factors for which β-catenin acts as a transcriptional coactivator, enhancing the expression of common target genes[8]. However, the possible physiological relevance of the crosstalk between FOXO3a and β-catenin in cancer has not been addressed.

FOXO proteins control multiple processes in eukaryotic organisms by regulating the expression of specific sets of genes involved in stem-cell maintenance, stress resistance, longevity, differentiation or metabolism[9,10]. In cancer, FOXO transcription factors are considered to be tumor suppressors because they induce cell-cycle arrest and apoptosis[11].

[1]Vall d'Hebrón Institut d'Oncología (VHIO), Stem Cell and Cancer Laboratory, Barcelona, Spain. [2]Instituto de Investigaciones Biomédicas 'Alberto Sols', Consejo Superior de Investigaciones Científicas-Universidad Autónoma de Madrid, Madrid, Spain. [3]Department of Pathology, Hospital Universitari Vall d'Hebrón, Universitat Autònoma de Barcelona, Barcelona, Spain. [4]Group of Drug Delivery and Targeting, Centro de Investigaciones en Bioquímica y Biología Molecular (CIBBIM)–Nanomedicine and Networking Biomedical Research Center on Bioengineering, Biomaterials and Nanomedicine (CIBER-BBN), Hospital Universitari Vall d'Hebrón, Institut de Recerca Vall d'Hebrón, Universitat Autònoma de Barcelona, Barcelona, Spain. [5]Parc de Recerca Biomèdica de Barcelona (PRBB), Centre d´Imatge Molecular (CRC) Corporació Sanitària, Barcelona, Spain. [6]VHIO, Genomics Cancer Group, Barcelona, Spain. [7]Centre for Respiratory Research, Rayne Institute, University College London, London, UK. [8]Hematopoietic Stem Cell Laboratory, London Research Institute, Cancer Research UK, London, UK. [9]General Surgery Service, Hospital Universitari Vall d'Hebrón, Barcelona, Spain. [10]Massachusetts General Hospital Cancer Center, Harvard Medical School, Charlestown, Massachusetts, USA. [11]Howard Hughes Medical Institute, Chevy Chase, Maryland, USA. [12]Medical Oncology Department, Hospital Universitari Vall d'Hebrón, Barcelona, Spain. [13]Present address: Swiss Institute for Experimental Cancer Research, École Polytechnique Fédérale de Lausanne, Lausanne, Switzerland. [14]These authors contributed equally to this work. Correspondence should be addressed to H.G.P. (hgpalmer@vhio.net).

Received 22 July 2011; accepted 10 April 2012; published online 20 May 2012; doi:10.1038/nm.2772

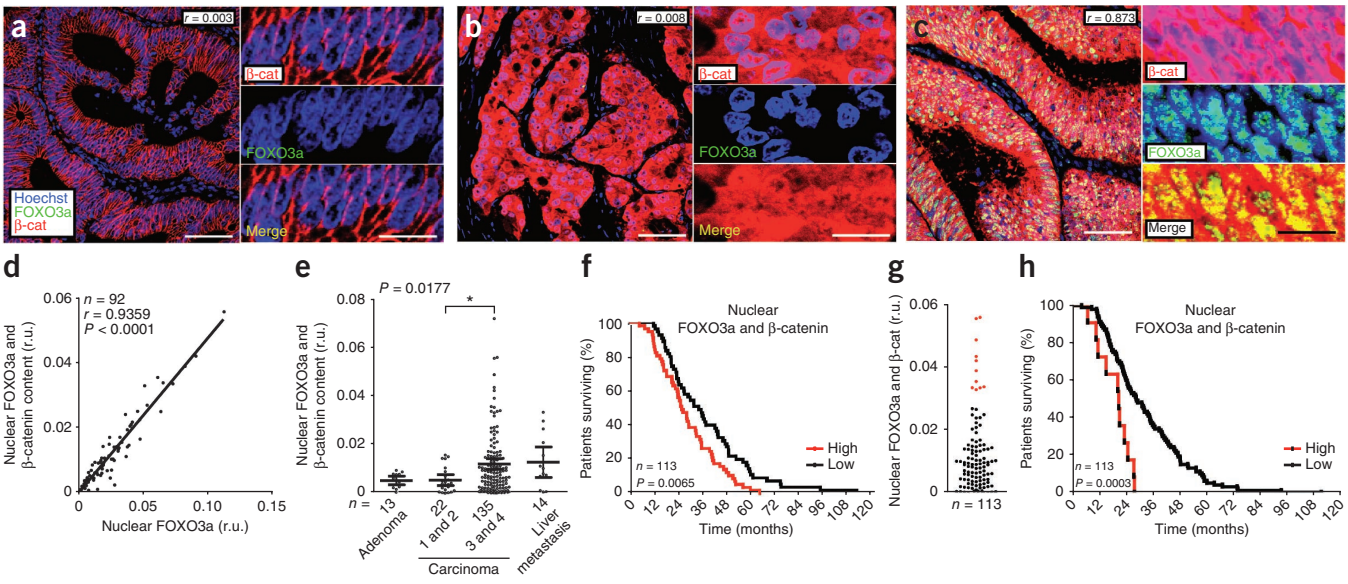

Figure 1 High nuclear concentrations of FOXO3a and β-catenin correlate with metastatic stage and shorter survival in patients with colon cancer. (**a**–**c**) Representative immunostained sections (left, scale bars, 100 μm) and the respective magnifications (right, scale bars, 20 μm) of tumors with low β-catenin (β-cat) and low FOXO3a expression (**a**), high β-catenin and low FOXO3a expression (**b**) and high β-catenin and high FOXO3a expression (**c**). FOXO3a is shown in green, β-catenin is shown in red, and Hoechst 33342 is shown in blue. The Spearman's coefficient of nuclear colocalization (*r*) is indicated (**b**,**c**). The merged magnified images lack blue channels, and yellow color indicates FOXO3a and β-catenin colocalization. (**d**) Plot depicting nuclear FOXO3a and β-catenin immunofluorescent signal intensity in human colon carcinomas. Correlation was evaluated by nonparametric Spearman test. The number of cases (*n*), coefficient of correlation (*r*) and *P* values are indicated. Relative units (r.u.) are calculated as described in the Online Methods. (**e**) Column scatter plot showing the amount of FOXO3a and β-catenin colocalization in tumors at different stages of colon-cancer progression. Horizontal lines indicate arithmetic mean values, and error bars show the 95% CI. The number of cases (*n*) and *P* values from nonparametric analysis of variance (ANOVA) analysis with Kruskal-Wallis test are indicated. Asterisk indicates a significant difference ($P < 0.05$) between groups as quantified by Dunn's multiple comparison test. (**f**) Kaplan-Meier survival analysis of patients with colon cancer separated into two groups by the median for the nuclear FOXO3a and β-catenin colocalization signal. The higher signal is shown in red ($n = 58$), and the lower signal is shown in black ($n = 55$). *P* values were calculated by log-rank (Mantel-Cox) test. (**g**) Plot representing the nuclear immunofluorescent signal for FOXO3a and β-catenin colocalization. Dots of the highest decile values are shown in red. (**h**) Kaplan-Meier survival analysis of patients with colon cancer separated into two groups by the highest decile for the nuclear FOXO3a and β-catenin colocalization signal. The higher signal is shown in red ($n = 11$), and the lower signal is shown in black ($n = 102$). *P* values were calculated by log-rank (Mantel-Cox) test.

Phosphorylation of FOXO proteins by activated v-akt murine thymoma viral oncogene homolog (AKT) or serum/glucocorticoid regulated kinase 1 (SGK1) induces their sequestration in the cytoplasm and the consequent inhibition of their transcriptional activity[12,13]. AKT is part of the rat sarcoma (RAS)-phosphoinositide-3-kinase (PI3K)-phosphatase and tensin homolog (PTEN)-AKT–mammalian target of rapamycin (mTOR) oncogenic pathway, which is frequently altered by activating mutations in colon and many other cancers[14]. Concerted efforts have been made in both academia and industry to identify specific anti-tumoral inhibitors of PI3K or AKT that relocate FOXO proteins back into the nucleus and thus restore their capacity to induce cell-cycle arrest and apoptosis[15]. In this study, we used the PI3K inhibitor NVP-BKM120 and the AKT signaling inhibitor-2 (API-2), which inhibit cell growth and induce apoptosis in human cancer cells in culture and in tumors growing in mice[16,17]. Phase 1 and 2 clinical trials with both compounds have been conducted in patients with solid metastatic cancers with promising results[18–20].

Considering the role of the Wnt–β-catenin and PI3K-AKT-FOXO3a pathways in tumorigenesis and the interaction of FOXO3a and β-catenin, we studied their crosstalk in colon cancer. We found that the joint action of the two transcription factors induced metastasis and that β-catenin conferred resistance to FOXO-induced apoptosis. Inhibitors of PI3K and AKT not only did not induce apoptosis *in vitro* or *in vivo*, but they also promoted metastasis when the concentration of nuclear β-catenin was high in colon-cancer cells. By studying the response of patient-derived colon-cancer–initiating cells to such target-directed drugs, we highlight the clinical relevance of our findings.

RESULTS

Nuclear FOXO3a and β-catenin concentrations in colon cancer

To assess the amount of nuclear FOXO3a and β-catenin in human colon cancer, we performed double immunofluorescent staining on paraffin sections of tumors at different stages. Nuclear FOXO3a accumulated alone in nonmalignant adenomas but always colocalized with β-catenin in the nuclei of tumoral cells in carcinomas and liver metastasis. We also detected carcinomas with high concentrations of nuclear β-catenin but low concentrations of nuclear FOXO3a. We found the highest nuclear concentrations of both factors in a subset of primary carcinomas at stages 3 or 4 from patients with metastatic disease (**Fig. 1a**–**e** and **Supplementary Fig. 1a**–**c**). Patients with high nuclear FOXO3a and β-catenin colocalization signals had, on average, an 8-month shorter survival time than patients with low colocalization signals. The median survival time was 33.7 months for patients with low nuclear FOXO3a and β-catenin signals and was 25.7 months for patients with high nuclear FOXO3a and β-catenin signals (hazard ratio (HR) 1.724, 95% CI 1.164–2.552). When we were more restrictive and analyzed the group of patients with the top 10% highest colocalization signals, the median survival was even shorter, 21.03 months, whereas it was 28.9 months for

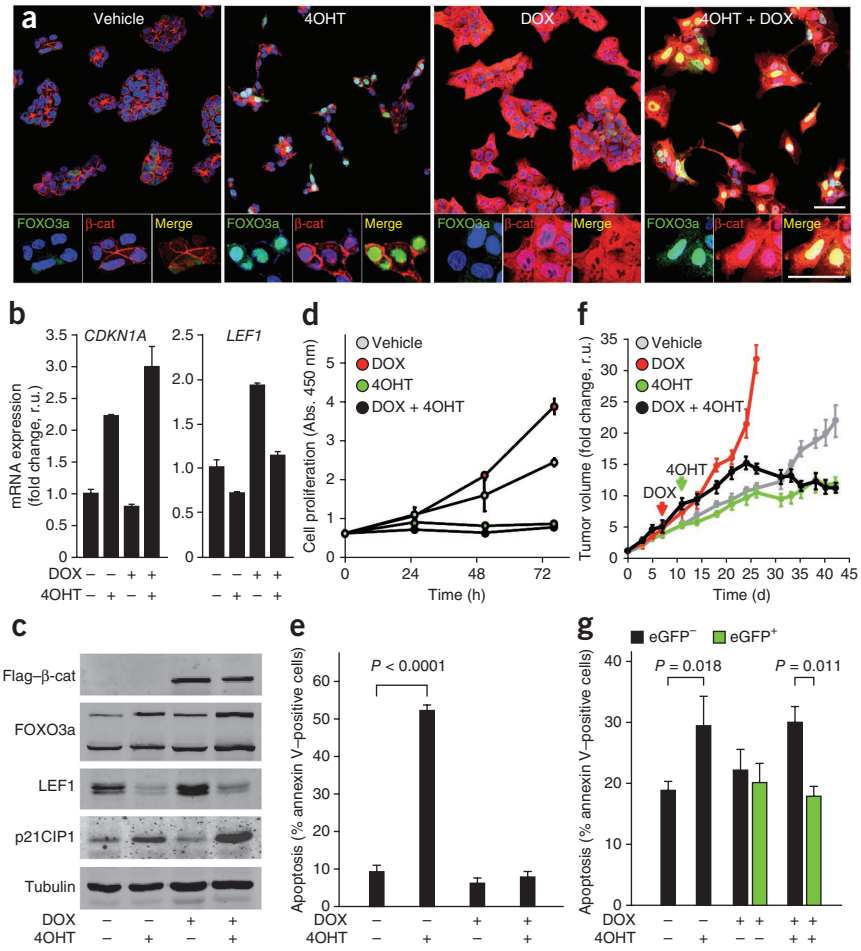

Figure 2 FOXO3a and β-catenin modulate colon cancer cell proliferation and apoptosis. (**a**) Immunofluorescence analysis of FOXO3a (green) and β-catenin (red) expression in DLD-1Fβ-C7 cells treated as indicated. Scale bar, top images, 50 μm. Below are magnifications of the upper images. Scale bar, bottom images, 20 μm. Nuclei were stained with Hoechst 33342 (blue). The merged magnification images lack the blue channel, and yellow color indicates FOXO3a and β-catenin colocalization. DOX, doxycycline. (**b**) Normalized relative *CDKN1A* and *LEF1* RNA expression levels in DLD-1Fβ-C7 cells treated with doxycycline, 4OHT or both measured by real-time RT-PCR. (**c**) The amounts of the indicated proteins in DLD-1Fβ-C7 cells as assessed by western blot. Flag-tag antibody detects exogenous Flag-tagged S33Y β-catenin. FOXO3a antibody recognizes endogenous protein (lower band) and FOXO3a3A-ER^{TM} fusion protein (upper band). Tubulin served as the loading control. (**d**) Graphic showing the proliferation of DLD-1Fβ-C7 cells treated as indicated. Abs., absorbance. (**e**) Chart depicting the percentage of apoptotic DLD-1Fβ-C7 cells in response to the indicated treatments as measured by flow cytometry. The *P* value corresponds to an unpaired *t* test. Error bars show ± s.d. of triplicates from three independent experiments (**b**,**d**,**e**). (**f**) Tumor growth in nude mice ($n = 8$, two tumors per mouse) injected subcutaneously with DLD-1Fβ cells and treated as indicated. Error bars show means ± s.d. of the volume of 16 tumors per treatment. (**g**) Graphic representing the percentage of apoptotic subpopulations positive (green bars) or negative for S33Y β-catenin–eGFP (black bars) of DLD-1Fβ cells in tumors ($n = 6$) growing in nude mice treated as indicated. Error bars show means ± s.d. of the volume of six tumors per treatment. *P* values correspond to unpaired *t* tests.

the other 90% of individuals who had lower colocalization signals (HR 6.392, 95% CI 2.322–17.6). Nuclear FOXO3a alone also correlated with metastatic stage and shorter median survival time (low FOXO3a content, 32.57 months, compared to high FOXO3a content, 25.37 months, HR 1.684, 95% CI 1.137–2.493). In contrast, β-catenin alone did not predict metastasis stage or survival time (HR 1.212, 95% CI 0.8331–1.765) (**Fig. 1f–h** and **Supplementary Fig. 1c–f**).

β-catenin diverts FOXO3a-induced apoptosis to metastasis

We expressed a tamoxifen-inducible (4-hydroxy-tamoxifen, 4OHT) AKT-insensitive mutant of FOXO3a (FOXO3a3A-ER^{TM})[21] and a stable β-catenin S33Y mutant that is inducible by doxycycline in a clone of DLD-1 human colon cancer cells (DLD-1Fβ-C7). The mutant β-catenin was expressed with a lentivirus, together with enhanced GFP (eGFP) using an internal ribosome entry site (IRES) (Online Methods). Exogenous FOXO3a and β-catenin proteins accumulated in the nucleus after the corresponding 4OHT or doxycycline treatments (**Fig. 2a** and **Supplementary Fig. 2**), reaching concentrations in the nucleus that were comparable to those caused by hydrogen peroxide, in the case of FOXO3a (**Supplementary Fig. 2a**,**b**,**d**), or, in the case of β-catenin, to those present in cancer cell lines with naturally occurring β-catenin accumulation, such as the HCT116 or SW480 human colon cancer cell lines (**Supplementary Fig. 2a**,**c**,**d**). β-catenin enhanced the induction of the known FOXO3a target gene *CDKN1A* (also known as p21CIP1) that resulted from treatment with 4OHT. Likewise, nuclear β-catenin accumulation resulting from doxycycline treatment induced the TCF target gene *LEF1*, whose expression was reduced by FOXO3a (4OHT) (**Fig. 2b**,**c**)[22,23]. FOXO3a alone reduced cell proliferation by accumulating cells in G1 phase of the cell cycle[24], whereas β-catenin alone increased cell proliferation. When both factors were expressed simultaneously in the nucleus, the cells had a reduced proliferation, similar to that seen with FOXO3a alone, indicating its dominant effect over β-catenin (**Fig. 2d** and **Supplementary Fig. 3a**,**b**). Separately, FOXO3a induced apoptosis, whereas β-catenin did not have a major effect. Nuclear accumulation of both factors resulted in a complete rescue of FOXO3a-induced apoptosis by β-catenin independently of proliferation, as this effect also occurred in cells arrested in G1 phase using pretreatment with mitomycin C (**Fig. 2e** and **Supplementary Fig. 3c–e**).

We injected a pool of DLD-1Fβ cells subcutaneously into nude mice that were all positive for FOXO3a3A-ER^{TM}, although only 62% of the mice expressed S33Y β-catenin and eGFP. This mixed pool of cells recapitulated a heterogeneity in the nuclear concentrations of β-catenin that was similar to that detected in human colon carcinomas (**Supplementary Figs. 4a–d** and **5a**,**b**). In mice treated with doxycycline, tumors accumulated high amounts of nuclear β-catenin and grew more rapidly, whereas those treated with 4OHT had increased nuclear FOXO3a content and grew more slowly compared to control

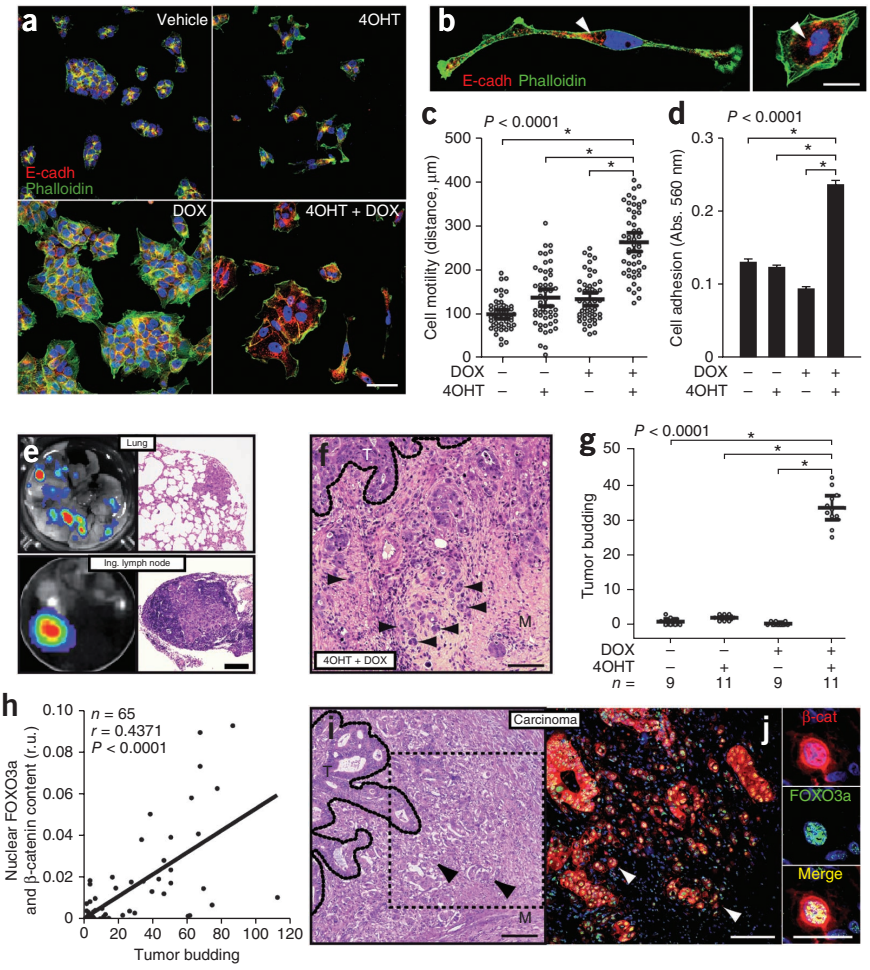

Figure 3 Nuclear FOXO3a and β-catenin drive cell scattering and metastasis. (**a**) Immunofluorescence analysis of DLD-1Fβ-C7 cells treated as indicated to detect E-cadherin (E-cadh) (red) and phalloidin-FITC–stained (phalloidin) actin filaments (green). Scale bar, 100 µm. (**b**) Immunofluorescence analysis of E-cadherin in DLD-1Fβ-C7 cells treated with 4OHT and doxycycline. Arrowheads indicate E-cadherin cytosolic aggregates. Scale bar, 10 µm. Nuclei were stained with Hoechst 33342 (blue; **a**,**b**). (**c**) Scatter plot representing the motility of DLD-1Fβ-C7 cells treated as indicated showing the distance covered by 50 individual cells in a time-lapse video recording one image every 20 min during 120 h. Horizontal bars indicate means, and error bars show the 95% CI. (**d**) Graphic representing adhesion to the substrate of DLD-1Fβ-C7 cells treated as indicated 5 min after seeding. Error bars show means ± s.d. of six replicates from two independent experiments. *P* values for non-parametric ANOVA analyses with Kruskal-Wallis test are shown. Asterisks indicate significant differences ($P < 0.0001$) between groups using Dunn's multiple comparison tests (**c**,**d**). (**e**) Bioluminescence imaging of organs obtained from necropsy of nude mice bearing orthotopic tumors from HT29Fβ cells injected in the cecum walls of the mice. Images overlaid with a gradual bioluminescent signal (blue to red) that originated from luciferase-expressing metastatic cells (left). H&E staining of the corresponding histological sections. Ing., inguinal. Scale bar, 100 µm. (**f**) H&E-stained histological section of the invasive front of a primary tumor xenograft from HT29Fβ cells growing in the cecum walls of nude mice treated with 4OHT and doxycycline described in **e**. Scale bar, 100 µm. (**g**) Column scatter plot presenting tumor budding in the primary tumors described in **e**. *n* indicates the number of tumors analyzed. Horizontal bars show the mean and the 95% CI. *P* values for non-parametric ANOVA analyses with Kruskal-Wallis test are shown. Asterisks indicate significant differences ($P < 0.0001$) between groups using Dunn's multiple comparison tests. (**h**) Dot plot representing the correlation of nuclear FOXO3a and β-catenin immunofluorescence signals with the incidence of tumor budding in 65 human primary colon carcinomas. Correlation was evaluated by non-parametric Spearman test, and *P* values were determined by non-parametric ANOVA analyses with a Kruskal-Wallis test. The number of cases (*n*), coefficient of correlation (*r*) and *P* values are indicated. Tumor budding and relative units (r.u.) of nuclear FOXO3a and β-catenin content were calculated as described in the Online Methods. (**i**) H&E-stained histological section of the invasive front of a primary human colon carcinoma. The black line delineates the tumor edge. T, tumor bulk; M, muscle. Black arrowheads indicate budding tumor cells. Scale bar, 100 µm. (**j**) Immunofluorescent staining of the invasive front of a human primary colon carcinoma for FOXO3a (green) and β-catenin (red). Nuclei were stained with Hoechst 33342 (blue). White arrowheads indicate budding tumor cells. The image on the left corresponds to the area in the dashed box in **i**, and on the right are magnifications. The merged magnified image lacks the blue channel, and yellow color indicates FOXO3a and β-catenin colocalization. Scale bar, left, 100 µm; right, 20 µm.

mice treated with vehicle (**Fig. 2f**). Combined treatment with doxycycline and 4OHT resulted in tumors with similar sizes at the end of the experiment as those treated with 4OHT alone. We observed that FOXO3a induced apoptosis only in DLD-1Fβ cells lacking β-catenin expression (eGFP$^-$ cells) both in culture and in xenograft tumors (**Fig. 2g** and **Supplementary Fig. 4e**). Within the tumor tissue, this resulted in high amounts of cell death, which was partially rescued by β-catenin expression (**Supplementary Fig. 5c**,**d**). We confirmed that nuclear accumulation of FOXO3a and β-catenin was significantly ($P < 0.0001$) increased as a result of treatment with 4OHT and doxycycline, respectively (**Supplementary Fig. 5e**,**f**).

Cells accumulating high amounts of both FOXO3a and β-catenin scattered and lost their epithelial phenotype in subconfluent cell cultures and *in vivo*. Nuclear FOXO3a alone also promoted a change in cell shape, but this phenotype is typical of the cell detachment associated with apoptosis (**Fig. 2a** and **Supplementary Figs. 5f** and **6a**). We detected relocation of E-cadherin protein from cell-to-cell contacts to cytoplasmic aggregates in cells in which FOXO3a and β-catenin induced this scattering phenotype (**Figs. 2a** and **3a**,**b** and **Supplementary Figs. 5f** and **6a**,**b**,**e**,**f**). We did not detect E-cadherin protein fragments, a repression of E-cadherin expression or an increase in the concentrations of Snail1, zinc finger E-box binding homeobox 1 (Zeb1) or Slug in these cells as a result of accumulation of FOXO3a, β-catenin or both. This ruled out E-cadherin proteolysis or the canonical epithelial-to-mesenchymal transition as mechanisms of the cell-to-cell detachment (**Supplementary Fig. 6c**,**d**). Further, these morphological changes correlated with increased cell motility and adhesion to substrate (**Fig. 3c**,**d** and **Supplementary Fig. 6e**–**g**). Although a small proportion of cells developed an increased size and extended cytoplasm that resembled the morphology of senescent cells, they were negative for senescence-associated β-galactosidase activity (**Fig. 2a** and **Supplementary Fig. 6b**,**f**,**h**).

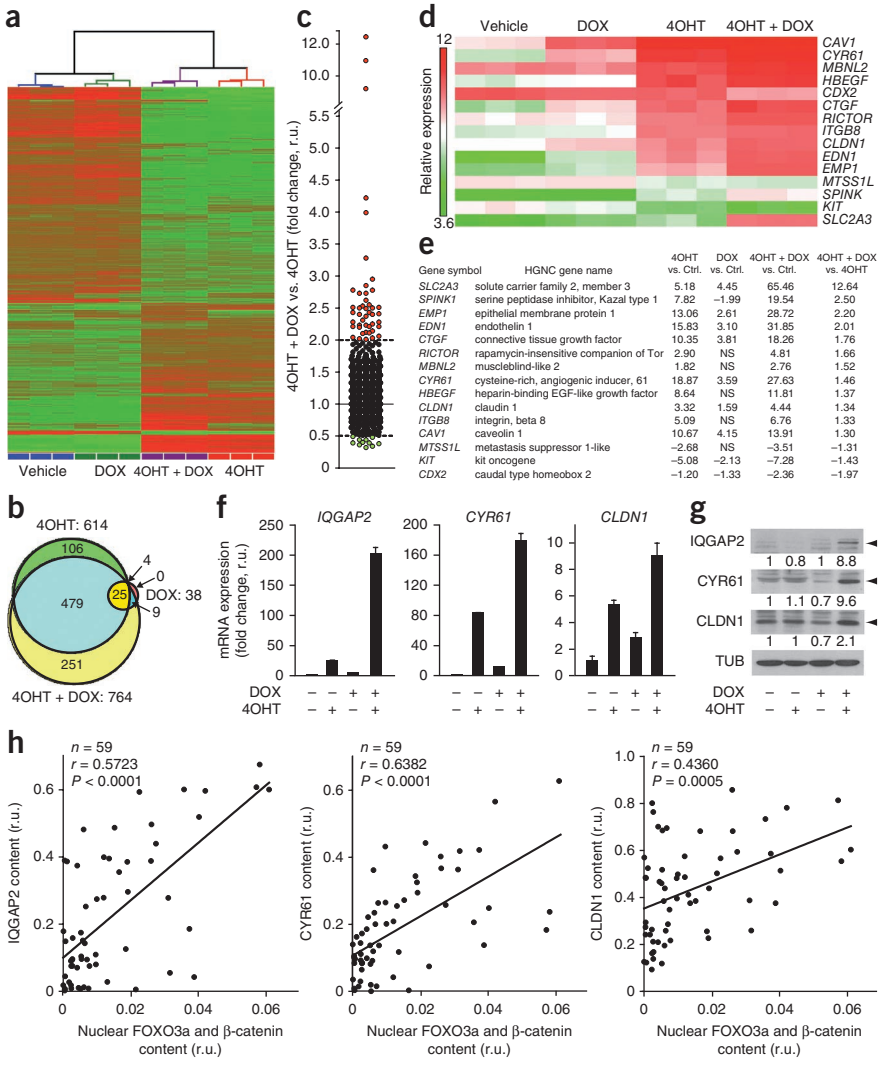

Figure 4 FOXO3a and β-catenin regulate a defined gene expression program. (**a**) Gene clustering diagram calculated using robust-multiarray–normalized expression values from the genome-wide microarray analysis. Triplicates of each treatment are indicated as colored rectangles at the bottom. Significance was calculated using two-tailed ANOVA with a significance cutoff of $P \leq 0.05$. Gene expression scaling, low (green) to high (red). (**b**) Venn diagram showing the number of genes regulated by the indicated treatments using a high-stringency analysis (with a Bonferroni cutoff $P \leq 0.05$) and having a twofold change compared to control in at least one of the conditions (**Supplementary Table 2**). (**c**) Plot representing changes in the relative expression of regulated genes comparing 4OHT and doxycycline with 4OHT alone. Red, higher than twofold induction; green, lower than twofold repression. (**d**) Metastasis signature. Heat map of robust-multiarray–normalized expression values for the genes involved in metastasis. Triplicates for each treatment are shown. Green, low expression; red, high expression. (**e**) Gene expression values of metastasis signature genes shown as a fold change compared to control vehicle-treated cells (Ctrl.) for the indicated treatments. The official gene symbols and HGNC gene names are listed. NS, not significant. (**f**) Mean relative mRNA expression levels of *IQGAP2, CYR61* and *CLDN1* transcripts measured by real-time RT-PCR in DLD-1Fβ-C7 cells after the indicated treatments. Error bars, triplicate values ± s.d. obtained in three independent experiments. (**g**) Western blot analysis of the indicated proteins in DLD-1Fβ-C7 cells. Numbers below the blot indicate the relative amount of each protein compared to the amount of the protein in vehicle-treated cells. All values are corrected by the respective tubulin signal that served as the loading control. (**h**) Dot plot showing the immunofluorescent signal intensity for each indicated protein correlated to the nuclear FOXO3a and β-catenin colocalization signal intensity in 59 human colon carcinomas. Correlation was evaluated by non-parametric Spearman test. The number of patients (n), coefficient of correlation (r) and P values are indicated. Relative units (r.u.) were calculated as described in the Online Methods.

We then tested the metastatic potential of cells expressing high amounts of nuclear FOXO3a and β-catenin, but no tumor was formed when we injected 1×10^6 DLD1-Fβ cells in the cecum walls of 50 nude mice. Thus, we engineered the same inducible systems to express exogenous FOXO3a and β-catenin as those used in DLD1-Fβ cells in human HT29 colon cancer cells (HT29Fβ). Treatment with doxycycline and 4OHT promoted equivalent effects on proliferation, apoptosis and cell scattering in HT29Fβ cells as those previously observed in DLD-1Fβ cells (**Supplementary Fig. 7**). We then injected HT29Fβ cells into the cecum walls of immunodeficient nude mice to assess whether the scattering phenotype induced by FOXO3a and β-catenin was indicative of an enhanced metastatic potential. We used a pool of these cells, all of which expressed FOXO3a3A-ER^{TM} and a luciferase reporter but only 41% of which contained the S33Y β-catenin–IRES-eGFP construct (Online Methods).

We observed an increase in tumor bioluminescent signal in immunodeficient nude mice treated with doxycycline that decreased or even disappeared in mice treated with 4OHT and that was weak in mice treated with both drugs together (**Supplementary Fig. 8a**,**b**). We performed exhaustive necropsies and *ex vivo* analyses of the internal organs of these mice using luminometry. We used histology to analyze tissues positive for bioluminescence to confirm metastases. We saw metastases in significantly more mice that had combined nuclear accumulation of FOXO3a and β-catenin than in any other group of mice in the experiment ($P = 0.022$), with the lungs being the most significant dissemination site of the metastases ($P = 0.038$) (**Fig. 3e** and **Supplementary Fig. 8c**,**d**). A control experiment conducted with parental luciferase-expressing HT29 cells that did not express exogenous FOXO3a or β-catenin did not show any such differences in metastasis frequencies after analogous 4OHT or doxycycline treatments (**Supplementary Fig. 8e**). Treatment with 4OHT induced nuclear FOXO3a accumulation, leading to marked intratumoral cell death, which was rescued by β-catenin (**Supplementary Fig. 9a**,**b**).

E-cadherin relocation, loss of epithelial organization and cell scattering occurred only in the cell population that was positive for the S33Y β-catenin–eGFP mutant in mice treated with both 4OHT and doxycycline (**Supplementary Fig. 9b–d**). Tumor budding was significantly increased in primary carcinomas growing in

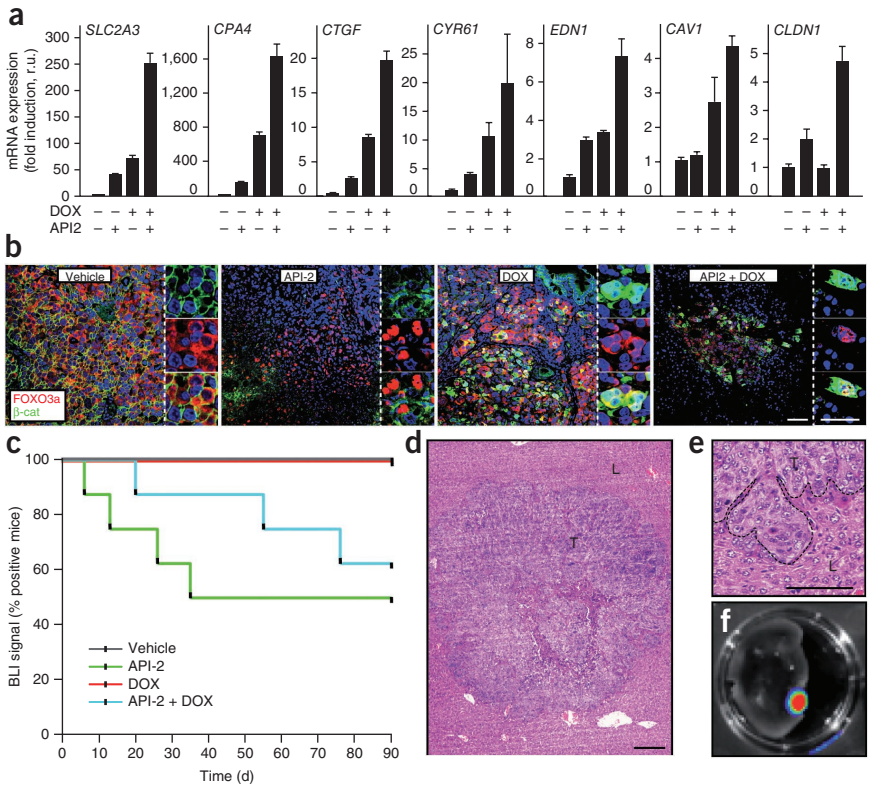

Figure 5 AKT inhibition by API-2 promotes metastasis of cells with high nuclear β-catenin content. (**a**) Relative mRNA levels of the indicated genes measured by real-time RT-PCR in DLD-1Fβ-C7 cells treated with API-2, doxycycline or both, as indicated. Error bars, ± s.d. of triplicates from three independent experiments. (**b**) Immunofluorescence analysis of FOXO3a (red) and β-catenin (green) expression in primary tumors growing in the cecum walls of nude mice. Scale bar, left images, 100 µm. Magnification of cells within the primary tumors (right). Scale bar, right images, 25 µm. Nuclei were stained with Hoechst 33342 (blue). (**c**) Kaplan-Meier analysis of bioluminescence (BLI) showing the percentage of nude mice injected in the cecum wall with HT29Fβ cells and treated as indicated that retained the signal over time. The number of mice used is listed in **Supplementary Table 5**. (**d**) H&E staining of liver metastasis from a cecum-injected mouse treated with API-2 and doxycycline. T, tumor; L, liver tissue. (**e**) A magnification of the image in **d** (top). The dashed line indicates the tumor-liver edge. *Ex vivo* image of infiltrated liver overlaid with gradual false-colored bioluminescent signal (blue, low; red, high) (bottom). Scale bar, **d**, 200 µm; **e**, 100 µm.

the cecum walls of mice treated with both 4OHT and doxycycline (**Fig. 3f**,**g**). We also found nuclear colocalization of FOXO3a and β-catenin in scattered cells at the invasive fronts of human colon carcinomas (**Fig. 3h–j**). By measuring the FOXO3a and β-catenin colocalization signal in the tumor bulk, we found that it had a positive correlation with tumor budding at the invasive front. Only a minor proportion of carcinomas had an increased accumulation of these factors at the invasive front, as has been previously described for β-catenin (**Supplementary Fig. 10**)[25].

FOXO3a and β-catenin co-regulate metastasis-relevant genes

Transcriptomic analyses showed that FOXO3a alone provoked a substantial change in the gene expression pattern of DLD-1Fβ cells[26], whereas β-catenin alone produced only a minor effect in these cells (**Fig. 4a**,**b** and **Supplementary Tables 1** and **2**). However, coexpression of β-catenin and FOXO3a enhanced the expression of many known or undescribed FOXO3a-induced target genes (**Fig. 4c**, **Supplementary Fig. 11a**,**b** and **Supplementary Tables 1** and **2**). In contrast, other genes involved in cell differentiation, such as *MUC13*, *VIL1* or *CDX2*, were repressed by nuclear FOXO3a, and the concomitant presence of nuclear β-catenin further enhanced such inhibition.

β-catenin enhances the expression of many FOXO3a target genes that are involved in cytoskeleton remodeling, cell shape and motility (**Supplementary Table 3**). The products of some of these genes are part of the protein complexes that control the stability of cell-to-cell contacts (**Supplementary Fig. 11c**,**d**)[27]. *IQGAP2* is one of these target genes that is involved in the stability of E-cadherin at adherent junctions[28,29]. The knockdown of IQGAP2 expression by shRNAi partially preserved the amount of E-cadherin that was associated with the actin cortex at cell-to-cell contacts in DLD1-Fβ-C7 cells treated with 4OHT and doxycycline. The induction of cell motility that was promoted by nuclear FOXO3a and β-catenin was also significantly reduced when we knocked down IQGAP2 (P = 0.0467). We also observed that IQGAP2 expression correlated with tumor budding in a set of 59 human colon carcinomas (**Supplementary Fig. 12**). We found IQGAP2 in association with E-cadherin aggregates in the cytoplasm of scattering DLD1-Fβ-C7 cells in culture or in subcutaneous xenografts as a result of FOXO3a and β-catenin nuclear colocalization and in cancer cells with disrupted epithelial organization in human colon carcinomas (**Supplementary Fig. 13**).

FOXO3a and β-catenin regulated a defined set of metastasis-relevant genes (**Fig. 4d**,**e** and **Supplementary Table 4**). In addition to *IQGAP2*, we also studied *CYR61* and *CLDN1*, which have both been reported to be associated with cell-to-cell disassembly and cell scattering, motility and metastasis[30,31]. The concentrations of nuclear FOXO3a alone or FOXO3a and β-catenin together correlated with the amount of protein expression of each of these three target genes in a set of 59 primary human colon carcinomas. The amount of nuclear β-catenin did not have any significant correlation with the protein expression of these genes (**Fig. 4f–h** and **Supplementary Figs. 14** and **15**).

A gene set enrichment analysis showed that FOXO3a regulated genes involved in apoptosis, whereas its coexpression with β-catenin also modulated genes controlling cell morphology, adhesion and motility. Nuclear β-catenin attenuated the upregulation of the proapoptotic genes *TNFSF10* and *BCL2L11*, and it synergized with FOXO3a to induce the upregulation of *FASLG* and the anti-apoptotic gene *HIPK3*. Moreover, β-catenin caused nuclear translocation of FAS-associated adaptor protein (FADD) and inhibited the poly (ADP-ribose) polymerase 1 (PARP1) cleavage that was induced by FOXO3a (**Supplementary Figs. 11a** and **16** and **Supplementary Table 3**).

AKT inhibition induces metastasis cooperating with β-catenin

The phosphorylation of FOXO3a by AKT translocates it from the nucleus to the cytoplasm. We therefore used the anti-tumoral drug API-2, which specifically inhibits AKT, to relocate FOXO3a back to

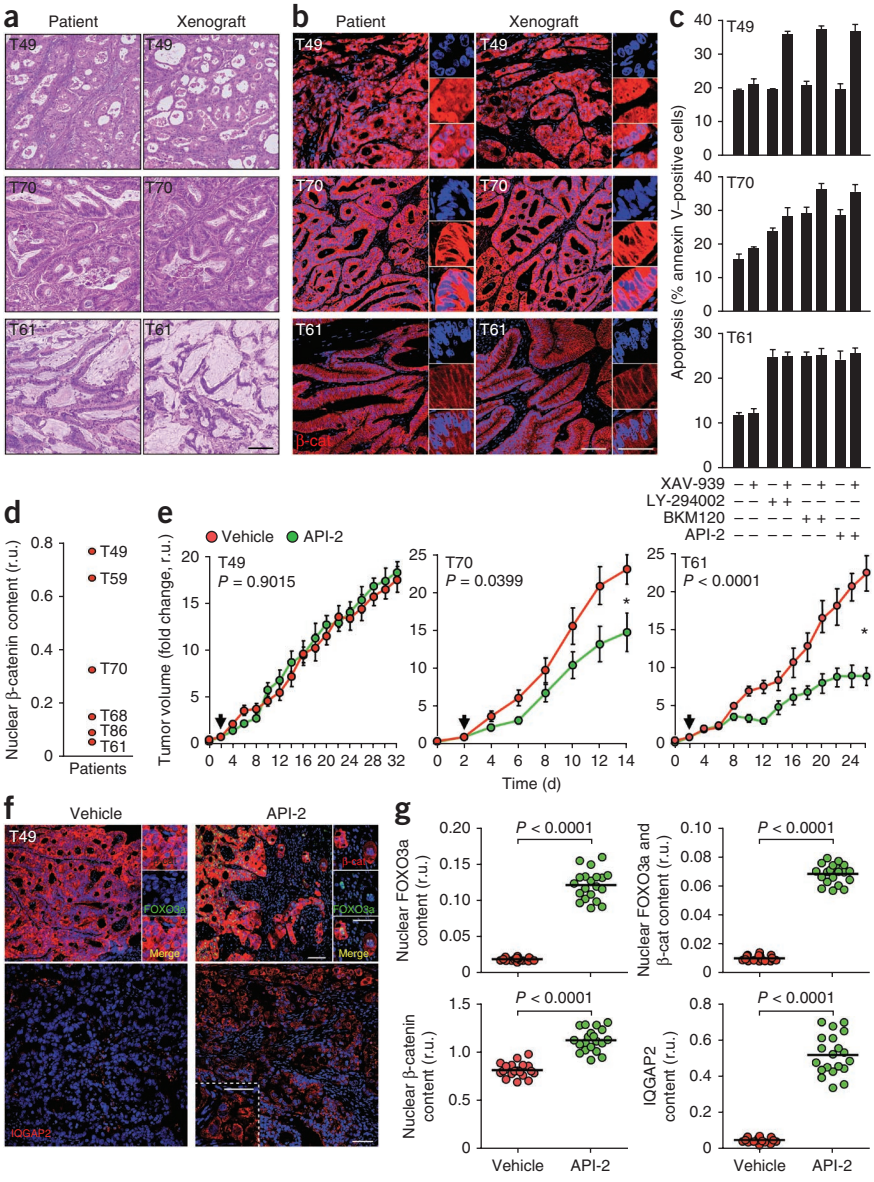

Figure 6 High nuclear β-catenin concentrations confer resistance to PI3K and AKT inhibitors in colon cancer patient-derived cells. (**a**) H&E staining of the primary carcinomas of the patients (left) and subcutaneous tumors (right, xenograft) generated in NOD-SCID mice from the corresponding patient-derived cells. Scale bar, 100 μm. (**b**) Immunofluorescent staining for β-catenin (red) in the primary carcinomas of the patients (left) and the corresponding subcutaneous xenograft tumors in mice (right). The smaller images on the right correspond to magnifications that show the amount of nuclear β-catenin. Nuclei were stained with Hoechst 33342 (blue). Scale bar, left images, 100 μm; right images, 50 μm. (**c**) Percentages of apoptotic cells in patient-derived sphere cultures treated as indicated. Apoptosis was measured by flow cytometry. Bars represent the mean of three independent experiments. Error bars, ± s.d. Cells were treated with the indicated compounds as described in the Online Methods. (**d**) Graph showing the amount of nuclear β-catenin measured by immunofluorescence in the primary colon carcinomas of each indicated patient. Relative units (r.u.) were calculated as described in the Online Methods. (**e**) Cancer cells derived from tumors from the three indicated patients were injected subcutaneously in NOD-SCID mice and treated with API-2 or vehicle ($n = 5$, two flanks per mouse). Arrows mark the initiation of treatment. The represented fold change was calculated by comparing the tumor volume at each given time point to the volume at the first day of treatment. Relative units (r.u.) were calculated as described in the Online Methods. Error bars, ± s.d. of ten tumors per treatment. *P* values correspond to non-parametric Mann-Whitney test. Asterisks indicate significant differences (with the *P* values indicated on the graphs) between the volumes of the tumors growing in mice treated with vehicle compared to mice treated with API-2. (**f**) Immunofluorescent staining for FOXO3a (green) and β-catenin (red) in histological sections of subcutaneous xenografted tumors from patient T49 treated as indicated (top images). The images on the right are magnifications that show the amounts of nuclear FOXO3a and β-catenin. Scale bar, left images, 100 μm; right images, 50 μm. Immunofluorescent staining for IQGAP2 (red) in the same xenograft tumors (bottom images). The insert shows a magnification of the cells with IQGAP2 accumulated in their cytoplasmic aggregates. Scale bar, main images, 100 μm; insert, 50 μm. Nuclei were stained with Hoechst 33342 (blue). (**g**) Column scatter plots showing the expression of each indicated protein in xenografted tumors from patient T49 treated as labeled. Five images were quantified for each of the four tumors treated. *P* values correspond to non-parametric Mann-Whitney test comparing the values of protein expression in each quantified picture. Relative units (r.u.) were calculated as described in the Online Methods.

the nucleus. Nuclear FOXO3a accumulation resulting from treatment with 4OHT or the AKT inhibitor API-2 promoted the scattering of DLD-1Fβ cells when concomitant high nuclear concentrations of β-catenin were induced by doxycycline. Some of the FOXO3a and β-catenin target genes defined in our metastasis signature were induced by API-2 and were further enhanced by β-catenin in DLD1-Fβ-C7 cells (**Figs. 4d**,**e** and **5a** and **Supplementary Fig. 17b**,**c**).

In tumors of HT29Fβ cells growing in the cecum walls of nude mice, treatment with API-2 and doxycycline induced the nuclear accumulation of FOXO3a and β-catenin, respectively, as well as the loss of the epithelial phenotype and the promotion of cell scattering (**Fig. 5b** and **Supplementary Fig. 17a**). Most crucially, although API-2 treatment reduced the primary tumor bioluminescence signal, it simultaneously promoted the development of metastasis when nuclear β-catenin was expressed. A significantly higher number of mice had metastases when treated with both API-2 and doxycycline compared to mice treated with vehicle ($P = 0.015$) (**Fig. 5c** and **Supplementary Table 5**). We found more mice affected in the lungs or lymph nodes or that had carcinomatosis as a result of treatment with both API-2 and doxycycline than as a result of vehicle treatment. Notably, API-2 treatment produced liver metastasis when β-catenin concentrations were high. We never detected this dissemination site previously in our HT29Fβ-cell model, and this site recapitulated the main organ affected in human patients with colon cancer (**Fig. 5d–f**).

β-catenin confers resistance to PI3K and AKT inhibitors

We observed a dose-dependent resistance to API-2–induced apoptosis that correlated with nuclear β-catenin content in DLD-1Fβ-C7 cells. HCT-116F cells with high endogenous amounts of mutant nuclear β-catenin or HT29Fβ cells with medium amounts were more resistant to NVP-BKM120– and API-2–induced apoptosis than DLD-1Fβ cells with any amount of nuclear β-catenin (**Supplementary Figs. 17b–h** and **18a**,**b** and **Supplementary Table 6**). In L8 colon cancer cells that are heterogeneous with respect to nuclear β-catenin concentrations and transcriptional activity, LY-249002, a pharmacological inhibitor of PI3K, preferentially induced apoptosis in the cell population with low expression of β-catenin (**Supplementary Fig. 19a–c**). Notably, the tankyrase inhibitor XAV-939, which reduces nuclear β-catenin concentrations and transcriptional activity, increased the sensitivity of HCT-116F cells to NVP-BKM120– and API-2–induced apoptosis (**Supplementary Figs. 17d**,**e**, **18b** and **19d–f**)[32].

We also analyzed the response to treatment of patient-derived colon cancer cells. Corresponding sphere cultures can regenerate carcinomas that preserve the same amounts of nuclear β-catenin and are histologically indistinguishable from the primary tumors of the patients after subcutaneous injection in nonobese diabetic severe combined immunodeficient (NOD-SCID) mice (**Fig. 6a**,**b** and **Supplementary Fig. 18c**,**d**). Treatment of sphere cultures with LY-294002 or NVP-BKM120 and API-2 induced the nuclear accumulation of FOXO3a and apoptosis in cells derived from patients T61, T68, T70 and T86, who originally presented with low nuclear β-catenin concentrations in their primary carcinomas. In contrast, sphere cultures derived from patients T49 and T59, who had high nuclear β-catenin concentrations, were innately resistant to the cell death mediated by these drugs. Notably, reduction of β-catenin concentrations by XAV-939 reverted such resistance (**Fig. 6c**,**d** and **Supplementary Fig. 18e–g**). In contrast, the sphere cultures were resistant to conventional chemotherapeutic agents such as 5-fluorouracil (5-FU) or oxaliplatin, and a combination treatment with these agents and XAV-939 did not sensitize the cultures to apoptosis (**Supplementary Fig. 18h**).

In vivo, treatment with API-2 inhibited the growth of the subcutaneous tumors generated in NOD-SCID mice when they were injected with cells derived from patient T61 (low β-catenin concentration), whereas mice injected with cells derived from patient T70 (intermediate β-catenin concentration) had only a partial response to API-2, and mice injected with cells derived from patient T49 (high β-catenin concentration) were resistant to API-2 treatment (**Fig. 6d**,**e**). The reduction of S6 ribosomal protein phosphorylation confirmed the efficacy of API-2 treatment in inhibiting PI3K-AKT pathway signaling *in vivo* (**Supplementary Fig. 20).** An analysis of the xenograft tumor derived from patient T49 revealed that API-2 treatment induced nuclear FOXO3a accumulation and increased cytoplasmatic IQGAP2 concentrations in tumor cell populations with disrupted epithelial organization. We also observed an enrichment of cells with high nuclear β-catenin concentrations in API-2–treated xenograft tumors from patient T49 compared to vehicle-treated control tumors (**Fig. 6f**,**g**).

DISCUSSION

Metastases are responsible for over 90% of deaths in patients with cancer, but the molecular mechanisms that drive this process are not well understood. Our data reveal previously unknown mechanisms by which FOXO3a and β-catenin can induce metastasis independently of the corresponding upstream pathways that control their nuclear accumulation[13,33].

Whereas some findings have related an abnormal activation of the Wnt–β-catenin pathway to metastasis[34], the contribution of PI3K-AKT-FOXO signaling to this process is not clear. On the one hand, mutational activation of PI3K and induction of AKT activity mediate metastasis[35], which might encourage the use of therapeutic inhibitors of PI3K and AKT. On the other hand, AKT can inhibit cell motility by blocking the transcriptional activity of nuclear factor of activated T cells (NFAT)[36]. Our results, which show that AKT inhibitors promote metastasis resulting from nuclear FOXO3a accumulation and cooperation with β-catenin, support the second notion.

Few studies have correlated FOXO3a function with metastasis or poor prognosis in cancer[37,38]. On the contrary, most studies have defined FOXO proteins as tumor suppressors, as they induce cell-cycle arrest and apoptosis[9,11]. Indeed, the combined knockdown of FOXO1, FOXO3 and FOXO4 in mice is responsible for tumor initiation[39]. However, our results reveal a previously unknown role for FOXO3a as an inducer of metastasis when acting in concert with β-catenin. We observed that the simultaneous nuclear accumulation of FOXO3a and β-catenin in primary tumors correlated with stages 3 and 4 of local or distant metastases and significantly shorter overall survival time of patients with colon cancer.

We show that to acquire such metastatic capacity, FOXO3a and β-catenin regulate functional sets of common target genes that are involved in reorganizing the cytoskeleton, destabilizing cell-to-cell contacts and increasing cell motility and migration, angiogenesis or evasion of the immune system. In particular, we revealed *IQGAP2* as a new target gene of FOXO3a–β-catenin complex that is required for destabilizing E-cadherin–containing adherens junctions, cell scattering and motility in colon carcinomas, indicating its role in metastasis.

AKT inhibition by API-2 induces nuclear FOXO3a accumulation and, in concert with nuclear β-catenin, promotes the expression of the aforementioned metastasis-related target genes and metastasis in mice. In fact, the nuclear accumulation of both factors correlates with tumor budding in human colon carcinomas.

Drug resistance is another crucial clinical feature that determines tumor relapse and patient survival. In particular, the mechanisms underlying resistance to new PI3K or AKT inhibitors are largely unknown[18,40,41]. Part of the anti-tumoral action of PI3K and AKT inhibitors is based on nuclear FOXO accumulation and subsequent cell-cycle arrest and apoptosis[42]. We show that nuclear β-catenin activity acts as a new mechanism of resistance to the FOXO3a-induced apoptosis promoted by inhibitors of PI3K or AKT. Thus, the induction of FOXO3a proapoptotic target genes such as *TNFSF10* (encoding TRAIL) or *BCL2L11* (encoding BIM)[43] is reduced by nuclear β-catenin, whereas FOXO3a and β-catenin cooperate synergistically to induce the anti-apoptotic kinase homeodomain interacting protein kinase 3 (HIPK3), which is responsible for FADD phosphorylation and confers resistance to death-receptor–mediated apoptosis[44,45].

Colon carcinomas are heterogeneous tissues containing cell populations with diverse biological properties and various amounts of nuclear β-catenin[3,25,46,47]. Cells with high nuclear β-catenin content behave as cancer stem cells[48,49] and are resistant to the FOXO3a-induced apoptosis that is promoted by inhibitors of PI3K or AKT. This resistant behavior leads to relapse and metastasis by inducing FOXO3a and β-catenin common target genes, supporting the concept of metastatic cancer stem cells (**Supplementary Fig. 21**)[49–52]. Indeed, sphere cultures derived from patients with colon cancer, which are enriched in cancer stem cells and which originated from tumors with high nuclear β-catenin content, were resistant to PI3K and AKT inhibitors *in vitro* and in subcutaneous xenograft tumors.

The information provided by these sphere cultures highlights the validity of studying target-directed therapies in cells derived from colon tumors immediately after surgical resection, as patients could therefore benefit from a personalized, experiment-based decision on the optimal treatment method. In the particular case of PI3K or AKT inhibitors, undesirable induction of FOXO3a and β-catenin target genes and promotion of metastasis could be predicted and avoided.

We show that the tankyrase inhibitor XAV-939 (ref. 32) sensitizes resistant cells specifically to the FOXO3a-induced apoptosis that is promoted by PI3K or AKT inhibitors. In contrast, XAV-939 does not have any benefit when combined with conventional chemotherapeutic agents such as 5-FU or oxaliplatin in cultures of colon-cancer–initiating cells. This points to a valid strategy to overcome drug resistance and metastasis by combining PI3K or AKT and Wnt–β-catenin inhibitory drugs. Currently used Wnt signaling inhibitors have reduced activity *in vivo*, and a new generation of tankyrase inhibitors with satisfactory *in vivo* activity must be developed to translate our results to clinical practice.

The benefit of some PI3K and AKT inhibitors is currently being tested in clinical trials in patients with colon cancer with advanced metastatic disease[15], and these inhibitors may be tested as part of adjuvant therapy in the future. Our findings call for the measurement of nuclear β-catenin concentrations as a biomarker of response to treatments that provoke FOXO3a nuclear accumulation to predict apoptosis or metastasis. This would be advisable for PI3K and AKT inhibitors and may be extended to other drugs such as cetuximab or receptor tyrosine kinase inhibitors that act upstream of a common oncogenic pathway.

METHODS

Methods and any associated references are available in the online version of the paper.

Note: Supplementary information is available in the online version of the paper.

ACKNOWLEDGMENTS

We thank W. Shao (Novartis Institutes for BioMedical Research, Inc.) for providing the experimental drug, XAV-939, and its inactive analog, LDW-643, and we thank K.F. Becker (Technische Universität München, Germany) for providing the antibody to Snail1. We also thank P.J. Coffer (Utrecht, Netherlands) for providing the pcDNA3-FOXO3a(A3):ER^{TM} expression plasmid, as well as H. Clevers (Utrecht, Netherlands) for providing L8 colon cancer cells. J. Seoane and G. Folch (VHIO, Barcelona, Spain) provided technical advice and reagents. We thank R. Luthra (Molecular Diagnostics Laboratory, MD Anderson Cancer Center, Houston, Texas, USA) for providing the CLIA panel of somatic mutations. We thank M.J. Larriba (Instituto de Investigaciones Biomédicas 'Alberto Sols', Consejo Superior de Investigaciones Científicas-Universidad Autónoma de Madrid, Madrid, Spain) for providing the reagents necessary for the analysis of Zeb1 and Slug expression and M. Scaltriti (Massachusetts General Hospital Cancer Center, Harvard Medical School, Charlestown, Massachusetts, USA) for supplying the lentiviruses used to knock down IQGAP2 expression. We acknowledge R. Rycroft and A. Wren for their valuable assistance in the preparation of the English version of the manuscript. Experiments were supported by a VHIO starting grant and grants from Fondo de Investigaciones Sanitarias–Instituto de Salud Carlos III (ISCIII) (FIS-PI081356, RETICC-RD06/0020/0075 and RETICC-RD06/0020/0009), and Plan Nacional de Biomedicina, Ministerio de Ciencia e Innovación (SAF-18302). S.P.T. was supported by a Fundació Olga Torres Fellowship, I.P. was funded by the Fundación Científica de la Asociación Española Contra el Cancer (AECC), and H.G.P. was supported by the Miguel Servet Program, ISCIII.

AUTHOR CONTRIBUTIONS

S.P.T., P.O.-M. and I.P. contributed equally to the experiments. S.P.T. also contributed to writing the manuscript, and I.C. also performed experiments. O.A. helped to perform IQGAP2 knockdown experiments. S.L. classified human tumors according to histopathological criteria and built the tissue arrays. Y.F. performed and analyzed live imaging assays (IVIS), which were supervised by S.S. J.R.H., S.R. and J.D.G. participated in live imaging experiments. L.M. and A.V. performed mutational analysis of human colon carcinomas. S.A. cloned and tested lentiviral constructs. S.R.y.C. provided human specimens. E.E. performed surgery on patients with colon cancer. J.B. supervised the project. J.T. supervised the project and provided clinical follow up on all the patients included in the study. A.M. and H.G.P. wrote the manuscript and supervised the project. H.G.P. was responsible for designing all the experiments and analyzing and interpreting all data.

COMPETING FINANCIAL INTERESTS

The authors declare no competing financial interests.

Published online at http://www.nature.com/doifinder/10.1038/nm.2772.
Reprints and permissions information is available online at http://www.nature.com/reprints/index.html.

1. Jemal, A. *et al.* Global cancer statistics. *CA Cancer J. Clin.* **61**, 69–90 (2011).
2. Jänne, P.A. & Mayer, R.J. Chemoprevention of colorectal cancer. *N. Engl. J. Med.* **342**, 1960–1968 (2000).
3. Clevers, H. Wnt/β-catenin signaling in development and disease. *Cell* **127**, 469–480 (2006).
4. Reya, T. & Clevers, H. Wnt signalling in stem cells and cancer. *Nature* **434**, 843–850 (2005).
5. Pálmer, H.G. *et al.* Vitamin D(3) promotes the differentiation of colon carcinoma cells by the induction of E-cadherin and the inhibition of β-catenin signaling. *J. Cell Biol.* **154**, 369–387 (2001).
6. Olson, L.E. *et al.* Homeodomain-mediated β-catenin-dependent switching events dictate cell-lineage determination. *Cell* **125**, 593–605 (2006).
7. Pálmer, H.G., Anjos-Afonso, F., Carmeliet, G., Takeda, H. & Watt, F.M. The vitamin D receptor is a Wnt effector that controls hair follicle differentiation and specifies tumor type in adult epidermis. *PLoS ONE* **3**, e1483 (2008).
8. Essers, M.A. *et al.* Functional interaction between β-catenin and FOXO in oxidative stress signaling. *Science* **308**, 1181–1184 (2005).
9. Calnan, D.R. & Brunet, A. The FoxO code. *Oncogene* **27**, 2276–2288 (2008).
10. van der Horst, A. & Burgering, B.M. Stressing the role of FoxO proteins in lifespan and disease. *Nat. Rev. Mol. Cell Biol.* **8**, 440–450 (2007).
11. Myatt, S.S. & Lam, E.W. The emerging roles of forkhead box (Fox) proteins in cancer. *Nat. Rev. Cancer* **7**, 847–859 (2007).
12. Brunet, A. *et al.* Akt promotes cell survival by phosphorylating and inhibiting a Forkhead transcription factor. *Cell* **96**, 857–868 (1999).
13. Dehner, M., Hadjihannas, M., Weiske, J., Huber, O. & Behrens, J. Wnt signaling inhibits Forkhead box O3a–induced transcription and apoptosis through up-regulation of serum- and glucocorticoid-inducible kinase 1. *J. Biol. Chem.* **283**, 19201–19210 (2008).
14. Walther, A. *et al.* Genetic prognostic and predictive markers in colorectal cancer. *Nat. Rev. Cancer* **9**, 489–499 (2009).
15. Dienstmann, R., Rodon, J., Markman, B. & Tabernero, J. Recent developments in anti-cancer agents targeting PI3K, Akt and mTORC1/2. *Recent Pat. Anticancer. Drug Discov.* **6**, 210–236 (2011).
16. Yang, L. *et al.* Akt/protein kinase B signaling inhibitor-2, a selective small molecule inhibitor of Akt signaling with antitumor activity in cancer cells overexpressing Akt. *Cancer Res.* **64**, 4394–4399 (2004).
17. Zheng, Y. *et al.* Novel phosphatidylinositol 3-kinase inhibitor NVP-BKM120 induces apoptosis in myeloma cells and shows synergistic anti-myeloma activity with dexamethasone. *J Mol Med (Berl)* (2011).
18. Liu, P., Cheng, H., Roberts, T.M. & Zhao, J.J. Targeting the phosphoinositide 3-kinase pathway in cancer. *Nat. Rev. Drug Discov.* **8**, 627–644 (2009).
19. Hoffman, K. *et al.* Phase I–II study: triciribine (tricyclic nucleoside phosphate) for metastatic breast cancer. *Cancer Chemother. Pharmacol.* **37**, 254–258 (1996).
20. Bendell, J.C. *et al.* Phase I, dose-escalation study of BKM120, an oral pan-class I PI3K inhibitor, in patients with advanced solid tumors. *J. Clin. Oncol.* **30**, 282–290 (2012).
21. Dijkers, P.F., Medema, R.H., Lammers, J.W., Koenderman, L. & Coffer, P.J. Expression of the pro-apoptotic Bcl-2 family member Bim is regulated by the forkhead transcription factor FKHR-L1. *Curr. Biol.* **10**, 1201–1204 (2000).
22. Seoane, J., Le, H.V., Shen, L., Anderson, S.A. & Massague, J. Integration of Smad and forkhead pathways in the control of neuroepithelial and glioblastoma cell proliferation. *Cell* **117**, 211–223 (2004).
23. Hoogeboom, D. *et al.* Interaction of FOXO with β-catenin inhibits β-catenin/T cell factor activity. *J. Biol. Chem.* **283**, 9224–9230 (2008).
24. Kops, G.J. *et al.* Forkhead transcription factor FOXO3a protects quiescent cells from oxidative stress. *Nature* **419**, 316–321 (2002).
25. Brabletz, T. *et al.* Variable β-catenin expression in colorectal cancers indicates tumor progression driven by the tumor environment. *Proc. Natl. Acad. Sci. USA* **98**, 10356–10361 (2001).
26. Delpuech, O. *et al.* Induction of Mxi1-SR α by FOXO3a contributes to repression of Myc-dependent gene expression. *Mol. Cell. Biol.* **27**, 4917–4930 (2007).
27. Wells, C.D. *et al.* A Rich1/Amot complex regulates the Cdc42 GTPase and apical-polarity proteins in epithelial cells. *Cell* **125**, 535–548 (2006).
28. Yamashiro, S., Abe, H. & Mabuchi, I. IQGAP2 is required for the cadherin-mediated cell-to-cell adhesion in *Xenopus laevis* embryos. *Dev. Biol.* **308**, 485–493 (2007).

29. Natale, D.R. & Watson, A.J. Rac-1 and IQGAP are potential regulators of E-cadherin-catenin interactions during murine preimplantation development. *Gene Expr. Patterns* **2**, 17–22 (2002).
30. Tsai, M.S., Hornby, A.E., Lakins, J. & Lupu, R. Expression and function of CYR61, an angiogenic factor, in breast cancer cell lines and tumor biopsies. *Cancer Res.* **60**, 5603–5607 (2000).
31. Dhawan, P. *et al.* Claudin-1 regulates cellular transformation and metastatic behavior in colon cancer. *J. Clin. Invest.* **115**, 1765–1776 (2005).
32. Huang, S.M. *et al.* Tankyrase inhibition stabilizes axin and antagonizes Wnt signalling. *Nature* **461**, 614–620 (2009).
33. Cross, D.A., Alessi, D.R., Cohen, P., Andjelkovich, M. & Hemmings, B.A. Inhibition of glycogen synthase kinase-3 by insulin mediated by protein kinase B. *Nature* **378**, 785–789 (1995).
34. Brabletz, T., Jung, A., Dag, S., Hlubek, F. & Kirchner, T. β-catenin regulates the expression of the matrix metalloproteinase-7 in human colorectal cancer. *Am. J. Pathol.* **155**, 1033–1038 (1999).
35. Samuels, Y. *et al.* Mutant PIK3CA promotes cell growth and invasion of human cancer cells. *Cancer Cell* **7**, 561–573 (2005).
36. Yoeli-Lerner, M. *et al.* Akt blocks breast cancer cell motility and invasion through the transcription factor NFAT. *Mol. Cell* **20**, 539–550 (2005).
37. Chen, J. *et al.* Constitutively nuclear FOXO3a localization predicts poor survival and promotes Akt phosphorylation in breast cancer. *PLoS ONE* **5**, e12293 (2010).
38. Storz, P., Doppler, H., Copland, J.A., Simpson, K.J. & Toker, A. FOXO3a promotes tumor cell invasion through the induction of matrix metalloproteinases. *Mol. Cell. Biol.* **29**, 4906–4917 (2009).
39. Paik, J.H. *et al.* FoxOs are lineage-restricted redundant tumor suppressors and regulate endothelial cell homeostasis. *Cell* **128**, 309–323 (2007).
40. Jun, T., Gjoerup, O. & Roberts, T.M. Tangled webs: evidence of cross-talk between c-Raf-1 and Akt. *Sci. STKE* **1999**, PE1 (1999).
41. Zunder, E.R., Knight, Z.A., Houseman, B.T., Apsel, B. & Shokat, K.M. Discovery of drug-resistant and drug-sensitizing mutations in the oncogenic PI3K isoform p110 α. *Cancer Cell* **14**, 180–192 (2008).
42. Gomes, A.R., Brosens, J.J. & Lam, E.W. Resist or die: FOXO transcription factors determine the cellular response to chemotherapy. *Cell Cycle* **7**, 3133–3136 (2008).
43. Obexer, P., Geiger, K., Ambros, P.F., Meister, B. & Ausserlechner, M.J. FKHRL1-mediated expression of Noxa and Bim induces apoptosis via the mitochondria in neuroblastoma cells. *Cell Death Differ.* **14**, 534–547 (2007).
44. Rochat-Steiner, V. *et al.* FIST/HIPK3: a Fas/FADD-interacting serine/threonine kinase that induces FADD phosphorylation and inhibits fas-mediated Jun NH(2)-terminal kinase activation. *J. Exp. Med.* **192**, 1165–1174 (2000).
45. Tourneur, L. & Chiocchia, G. FADD: a regulator of life and death. *Trends Immunol.* **31**, 260–269 (2010).
46. Shackleton, M., Quintana, E., Fearon, E.R. & Morrison, S.J. Heterogeneity in cancer: cancer stem cells versus clonal evolution. *Cell* **138**, 822–829 (2009).
47. Fodde, R. & Brabletz, T. Wnt/β-catenin signaling in cancer stemness and malignant behavior. *Curr. Opin. Cell Biol.* **19**, 150–158 (2007).
48. Clevers, H. The cancer stem cell: premises, promises and challenges. *Nat. Med.* **17**, 313–319 (2011).
49. Vermeulen, L. *et al.* Wnt activity defines colon cancer stem cells and is regulated by the microenvironment. *Nat. Cell Biol.* **12**, 468–476 (2010).
50. Brabletz, T., Jung, A., Spaderna, S., Hlubek, F. & Kirchner, T. Opinion: migrating cancer stem cells—an integrated concept of malignant tumour progression. *Nat. Rev. Cancer* **5**, 744–749 (2005).
51. Todaro, M. *et al.* Colon cancer stem cells dictate tumor growth and resist cell death by production of interleukin-4. *Cell Stem Cell* **1**, 389–402 (2007).
52. Van der Flier, L.G. *et al.* The intestinal Wnt/TCF signature. *Gastroenterology* **132**, 628–632 (2007).

ONLINE METHODS

Cell culture. Cell lines were cultured under standard conditions. DLD-1F cells are DLD-1 derivates expressing pcDNA-FOXO3a(3A)ER^{TM} (ref. 21). HT29F and HCT-116F cells express pLHCX-HA-FOXO3a(3A):ER^{TM}. HT29F cells additionally carry pGL4.51(luc2/CMV/Neo) (Promega). pSIN-TRE-Flag-β-catenin^{S33Y}-IRES-GFP–inducible lentivirus was used to generate DLD-1Fβ and HT29Fβ cells. Cell migration was quantified using time-lapse microscopy (3 frames per h for 120 h) using the cell-tracking plugin (ImageJ software). All parental cell lines were originally obtained from American Type Culture Collection.

Patient-derived cells. Primary colon-cancer cells were obtained from the adenocarcinomas of the patients immediately after surgery, as described[53]. Written informed consent was signed by all patients. The project was approved by the Research Ethics Committee of the Vall d'Hebron University Hospital, Barcelona, Spain (approval ID, PR(IR)79/2009).

Mice, xenotransplantation and bioluminescence. Experiments were conducted following the animal care directive of the European Union (86/609/EEC) and were approved by the Ethical Committee of Animal Experimentation of Vall d'Hebron Institute of Research (approval ID, 40/08 CEEA and 47/08/10 CEEA). Colon-cancer cells were orthotopically transplanted in the cecum walls of female NOD-SCID mice as previously described[54]. Doxycycline (2 mg/ml; Sigma-Aldrich) was administered *ad libitum* in drinking water containing 5% sucrose (Sigma-Aldrich). 4OHT (100 µg per dose, 1 µg/µl in sesame oil; Sigma-Aldrich) and API-2 (1 mg/kg in PBS and 2% DMSO; Tocris Bioscience) were injected intraperitoneally every other day. Bioluminescence imaging was performed with the IVIS Spectrum Imaging System (Caliper Life Sciences).

Mutational status of patient-derived cells and cancer cell lines. Samples were genotyped for 740 cancer-related mutations in 57 genes. OncoCarta (Sequenom), CLIA (MD Anderson Cancer Center, Houston, Texas) and VHIO-Card panels of somatic mutations (**Supplementary Table 7**) were analyzed with a MassARRAY spectrometer (Sequenom). Mutation data were from the COSMIC database (www.sanger.ac.uk/cosmic).

Western blot, histology and immunofluorescence. Tumor budding was quantified as described[55]. Western blot and immunofluorescence were performed as described[56]. The antibodies used are listed in **Supplementary Table 8**. The fluorescence images were analyzed with the MBF ImageJ for Microscopy program (www.macbiophotonics.ca) using criteria described earlier[56,57].

Flow cytometry. The proportions of apoptotic cells were determined using the annexin V–eGFP (GenScript), annexin V–phycoerythrin (PE) (BD Pharmingen) or annexin V–allophycocyanin (APC) (Bender MedSystems) kits. Anti-human TRA-85–APC staining (R&D Systems) discriminated cells between the species when analyzing human xenograft tumors growing in mice. Dead cells were detected by propidium iodide or DAPI staining.

Quantitative RT-PCR and transcriptomics. Quantitative RT-PCR was done using the comparative C_T method as described using SYBR Green (Applied Biosystems) and specific primer pairs (**Supplementary Table 9a**), applying geNorm algorithms to select reference transcripts (*SDHA* and *PPIA*) to use the geometric means for normalization and to calculate normalized s.d. values[58]. The transcriptome of the DLD-1Fβ-C7 cells was determined on an Affymetrix Human Gene 1.1-ST Array. Raw and normalized Minimum Information About a Microarray Experiment (MIAME)-compliant microarray data were deposited at ARRAYEXPRESS (www.ebi.ac.uk/arrayexpress) under accession number E-MEXP-3262.

Plasmids. pSIN-TRE-Flag-β-catenin^{S33Y}-IRES-GFP is a derivate[59] of the pRRL-cPPT-hPGK-TMPrtTA-WPRE plasmid[60] that has human S33Y Flag–β-catenin cds introduced. pLHCX-HA-FOXO3a(A3):ER^{TM} is a derivate of the FOXO3a(A3):ER^{TM} (ref. 21) and pLHCX plasmid (Clontech). 7TGP was previously described[61]. pGIPZ-shRNAmir constructs were from Open Biosystems (**Supplementary Table 9b**).

Reagents and treatments. Unless specified otherwise, cells were treated as follows: 2.5 µg/ml doxycycline for 36 h (Sigma-Aldrich), followed 12 h later with 50 nM 4OHT for 24 h (Sigma-Aldrich). Cells were also treated with 3.3 µM XAV-939 or LDW-643 (Novartis) for 120 h, followed 48 h later with 20 µM LY-294002 (Merck), 20 µM API-2 (Tocris Bioscience), 0.8 µM NVP-BKM120 (Selleck Chemicals), 50 µg/ml 5-FU (Sigma-Aldrich) or 100 µM oxaliplatin (Sigma-Aldrich) for 72 h. LDW-643 is an analog of XAV-939 with no activity and was used as a control. Cells were treated with 10 µg/ml mitomycin C for 3 h (Sigma-Aldrich), before 4OHT or doxycycline addition. Primary fibroblasts were treated with 0.1 µM doxorubicin (Sigma-Aldrich) for 24 h to induce senescence. Hoechst 33342 was used at a dose of 5 µg/ml (Sigma-Aldrich).

Viral infection. Lentiviral or retroviral particles were produced in 293T cells using standard procedures and psPAX2 and pMD2.G (Addgene) or pCL-Ampho (Imgenex Corp.) packaging vectors, respectively.

Statistics. Any $P < 0.05$ were considered statistically significant. We calculated correlation coefficients (r) using two-tailed nonparametric Spearman tests, which make no assumption about the distribution of the values, to compare the fluorescent signal values of different proteins, subcellular protein colocalization or tumor budding in tissue sections of human carcinomas. We used the nonparametric Kruskal-Wallis test to compare three or more groups of unpaired values that did not follow any particular distribution. This applied, for example, to measurements of protein colocalization in human carcinomas at different tumor stages and in comparing different treatments in cell motility and adhesion assays, as well as in quantifying tumor budding in orthotopically growing tumors. Then, Dunn's multiple comparison post-test was used to identify differences in the sum of ranks between each pair of groups of values. We analyzed the survival of the patients using the Kaplan-Meier method and compared the curves using a log-rank (Mantel-Cox) test assuming that the hazard function was the same at all times. We used the nonparametric Mann-Whitney test to compare unmatched groups of values corresponding to xenograft tumor volumes or luminescence signals, tissue protein expression and cell motility. Differences in apoptosis were analyzed by an unpaired t test comparing the means of two groups of values. We used Fisher's exact test to analyze the differences in incidence of metastasis compared to control.

53. Kreso, A. & O'Brien, C.A. Colon cancer stem cells. *Curr. Protoc. Stem Cell Biol.* **7**, 3.1.1–3.1.12 (2008).
54. Céspedes, M.V. *et al.* Orthotopic microinjection of human colon cancer cells in nude mice induces tumor foci in all clinically relevant metastatic sites. *Am. J. Pathol.* **170**, 1077–1085 (2007).
55. Ueno, H., Murphy, J., Jass, J.R., Mochizuki, H. & Talbot, I.C. Tumour 'budding' as an index to estimate the potential of aggressiveness in rectal cancer. *Histopathology* **40**, 127–132 (2002).
56. Barbáchano, A. *et al.* SPROUTY-2 and E-cadherin regulate reciprocally and dictate colon cancer cell tumourigenicity. *Oncogene* **29**, 4800–4813 (2010).
57. Arques, O., Chicote, I., Tenbaum, S., Puig, I. & Palmer, H.G. Standardized relative quantification of immunofluorescence tissue staining. *Protoc. Exchange* published online, doi:10.1038/protex.2012.008 (2 April 2012).
58. Vandesompele, J. *et al.* Accurate normalization of real-time quantitative RT-PCR data by geometric averaging of multiple internal control genes. *Genome Biol.* **3**, RESEARCH0034 (2002).
59. Aguilar, S. *et al.* Bone marrow stem cells expressing keratinocyte growth factor via an inducible lentivirus protects against bleomycin-induced pulmonary fibrosis. *PLoS ONE* **4**, e8013 (2009).
60. Barde, I. *et al.* Efficient control of gene expression in the hematopoietic system using a single Tet-on inducible lentiviral vector. *Mol. Ther.* **13**, 382–390 (2006).
61. Fuerer, C. & Nusse, R. Lentiviral vectors to probe and manipulate the Wnt signaling pathway. *PLoS ONE* **5**, e9370 (2010).